Science of the Total Environment 524–525 (2015) 427–439

Contents lists available at ScienceDirect

Science of the Total Environment

journal homepage: www.elsevier.com/locate/scitotenv

Spatial resolution of anthropogenic heat fluxes into urban aquifers

Susanne A. Benz [a,*], Peter Bayer [b], Kathrin Menberg [a,c], Stephan Jung [a], Philipp Blum [a]

[a] Karlsruhe Institute of Technology (KIT), Institute for Applied Geosciences (AGW), Kaiserstr. 12, 76131 Karlsruhe, Germany
[b] ETH Zurich, Department of Earth Sciences, Sonneggstr. 5, 8092 Zurich, Switzerland
[c] University of Cambridge, Department of Engineering, Trumpington Street, Cambridge, CB2 1PZ, United Kingdom

HIGHLIGHTS

- A spatially resolved model of subsurface anthropogenic heat fluxes is developed.
- The most dominant local heat fluxes are caused by district heating networks.
- Heat flow mainly stems from buildings and elevated ground surface temperatures.
- The thermal gradient of the unsaturated zone greatly impacts the heat fluxes.
- Subsurface anthropogenic heat fluxes provide a sustainable geothermal potential.

GRAPHICAL ABSTRACT

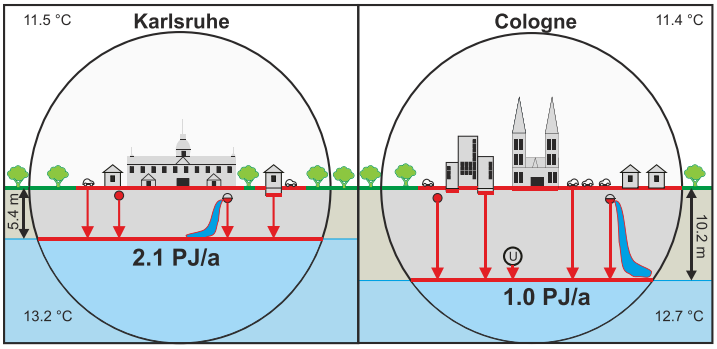

ARTICLE INFO

Article history:
Received 28 January 2015
Received in revised form 1 April 2015
Accepted 1 April 2015
Available online xxxx

Editor: D. Barcelo

Keywords:
Urban heat island
Heat flux
Groundwater temperatures
Anthropogenic heat flux
Urban energy balance

ABSTRACT

Urban heat islands in the subsurface contain large quantities of energy in the form of elevated groundwater temperatures caused by anthropogenic heat fluxes (AHF_S) into the subsurface. The objective of this study is to quantify these AHF_S and the heat flow they generate in two German cities, Karlsruhe and Cologne. Thus, statistical and spatial analytical heat flux models were developed for both cities. The models include the spatial representation of various sources of AHF_S: (1) elevated ground surface temperatures, (2) basements, (3) sewage systems, (4) sewage leakage, (5) subway tunnels, and (6) district heating networks. The results show that the district heating networks induce the largest AHF_S with values greater than 60 W/m^2 and one order of magnitude higher than fluxes from other sources. A covariance analysis indicates that the spatial distribution of the total flux depends mainly on the thermal gradient in the unsaturated zone. On a citywide scale, basements and elevated ground surface temperatures are the dominant sources of heat flow. Overall, 2.1 PJ/a and 1.0 PJ/a of heat are accumulated on average in Karlsruhe and the western part of Cologne, respectively. Extracting this anthropogenically originated energy could sustainably supply significant parts of the urban heating demand. Furthermore, using this heat could also keep groundwater temperatures from rising further.

© 2015 Elsevier B.V. All rights reserved.

1. Introduction

A warming of urban areas can be observed worldwide (Oke, 1973). The Urban Heat Island (UHI) phenomenon, as it is called, exists in all diverse layers of a city: from atmosphere (Bowler et al., 2010; Jauregui, 1997; Santamouris et al., 2001) to surface (Li and Bou-Zeid, 2014; Peng et al., 2012) to groundwater (Beltrami et al., 2005; Menberg et al., 2013a,b; Taniguchi et al., 2007). While various unfavorable issues such as increased mortality rates during heat waves (Gabriel and Endlicher, 2011) and regional atmospheric pollution (Sarrat et al., 2006) originate from the UHI in the atmosphere, the urban heat island

* Corresponding author.
E-mail addresses: susanne.benz@kit.edu (S.A. Benz), kcm30@cam.ac.uk (K. Menberg).

http://dx.doi.org/10.1016/j.scitotenv.2015.04.003
0048-9697/© 2015 Elsevier B.V. All rights reserved.

in the subsurface (SUHI) can be beneficial. The increased groundwater and subsurface temperatures provide economic and ecological advantages for the use of shallow geothermal energy systems located in SUHI (Allen et al., 2003). Arola and Korkka-Niemi (2014) showed that in southern Finland about 50–60% more peak heating power could be utilized from urban areas in contrast to rural areas. Furthermore, the geothermal potential of SUHI exceeds the annual residential heating demand in many urban areas (Zhu et al., 2010). Extracting this energy efficiently could save or even reduce CO_2 emissions and other greenhouse gases (Bayer et al., 2012; Blum et al., 2010). Hähnlein et al. (2013) conclude that a shallow geothermal system is only sustainable, if the generated energy is mainly renewable energy. Hence, energy sources of the SUHI should be evaluated and anthropogenic heat fluxes (AHF_S) into the subsurface of urban areas should be quantified.

Anthropogenic heat has long been discussed regarding the above ground UHI, where it describes the waste heat of human activities such as intense energy use, power generation and vehicular traffic (Taha, 1997). The anthropogenic heat flux in the atmosphere (AHF_A), for example, was simulated from global to city scale by Allen et al. (2011). Its impact on Tokyo was modeled by Ichinose et al. (1999), who found a 1 K temperature increase. For Chicago, San Francisco, Los Angeles, and Philadelphia, Sailor and Lu (2004) showed that the AHF_A on a citywide scale is between 10 and 80 W/m^2.

Urban heat islands in the subsurface (SUHI) have been observed in various cities worldwide such as Virginia Beach, USA (Eggleston and McCoy, 2014), Winnipeg, Canada (Ferguson and Woodbury, 2007), London, UK (Headon et al., 2009), Oberhausen, Germany (Muller et al., 2014), Istanbul, Turkey (Yalcin and Yetemen, 2009), Jakarta, Indonesia (Lubis et al., 2013), Osaka, Japan, and Bangkok, Thailand (Taniguchi et al., 2009). Some studies focus on the influence of rain and hydrological transport of heat (Kertesz and Sansalone, 2014; Kollet et al., 2009) on these thermal anomalies. In Cologne, Zhu et al. (2014) used a numerical flow and heat transport model to generate various groundwater temperature depth-profiles and compared them with measured profiles. It shows mechanisms such as vertical conductive heat input, horizontal advection and transverse dispersion to be the main thermal transport mechanisms. Overall, the consensus view is that anthropogenic heat is the dominant source of the SUHI.

Menberg et al. (2013b) define the anthropogenic heat flux (AHF_S) into the subsurface as the heat input into shallow urban aquifers caused by various anthropogenic heat sources. Previously they identified the following main anthropogenic heat sources: increased ground surface temperature (GST), buildings and basements, road tunnels, sewage networks, sewage leakages, district heating systems, subway systems, reinjections of thermal waste water and other geothermal energy systems such as ground source heat pump (GSHP) and groundwater heat pump systems (GWHP) (Menberg et al., 2013a).

In contrast, Hötzl and Makurat (1981) developed a first approach to quantify the heat flow balance of the SUHI in Karlsruhe. They identified solar irradiation, the geothermal heat flow, sewage and district heating networks, reinjection of thermal wastewater, and basements as possible heat sources. Furthermore, they estimated the amount of heat transported into the entire urban subsurface for each of these sources, identifying solar insolation and the sewage system to be the dominant heat sources. The revised model by Menberg et al. (2013b) includes elevated GST, buildings, reinjection of thermal wastewater, sewage network, sewage leakage, and district heating network as a source of anthropogenic heat. A regionalized anthropogenic heat flux model was introduced to account for the uncertainty of all parameters needed for an analytical solution. They performed one Monte Carlo simulation over the entire study area in which groundwater temperatures (GWT), groundwater depth, building density, and basement depth were linked to their spatial distribution. Thus, they were able to estimate the city-scale mean of all individual heat fluxes and the total amount of energy entering the aquifer. For both studied years, 1977 and 2011, elevated ground surface temperatures (GST) were the dominant heat source. Furthermore, a spatial analysis of heat fluxes from buildings was introduced, exhibiting a considerable range between -0.1 and >10 W/m^2. In Basel, Switzerland, Epting et al. (2013) used a numerical heat transport model to compare the cumulative heat fluxes in 2010 from natural and anthropogenic boundaries. They defined these anthropogenic boundaries as reinjection of thermal wastewater as well as small, large, and deep buildings. The absolute heat flux from these different types of buildings was determined to be 1.8×10^{-1} W/m^2, 3.0×10^{-11} W/m^2 and 16 W/m^2, respectively.

Although several previous studies analyzed various AHF_S, currently, there is no method available that gives a complete and detailed picture of the spatial distribution of AHF_S. However, in combination with aquifer scale models (e.g. central London, Herbert et al., 2013), the detailed spatial distribution of AHF_S is a crucial requirement for the development of a sustainable thermal energy management tool. The objective of the present study is therefore to introduce a method that quantifies the vertical AHF_S from various heat sources through the unsaturated zone into the groundwater and displays their spatial distribution. This two-dimensional approach builds up on the model framework developed by Menberg et al. (2013b); however, it separates spatial variability and uncertainty of the input parameters. Hence, a more accurate determination of heat fluxes is obtained. In addition, the heat flux model is applied in two German cities, Karlsruhe and Cologne, providing a comparison of the determined AHF_S. Finally, we investigate the possible implications of the AHF_S on thermal groundwater use by comparing the annual thermal recharge of AHF_S with the residential space heating demand to evaluate the potential of the SUHI as a sustainable source of thermal energy.

2. Material and methods

2.1. Study sites

The chosen study areas cover major parts of two German cities: Karlsruhe, located in the south-west of Germany close to the Rhine, and Cologne, located in the west of Germany next to the Rhine (Fig. 1). Both study sites are limited to areas dominated by urban land-use, i.e. mostly built-up areas, within the city districts. Large green spaces, such as woodlands and agricultural areas, at the borders of the city districts are not included in the investigations. In the following, the geology, hydrogeology, groundwater temperatures (GWT), and urban infrastructures of these cities are described. An overview and general statistics of both study areas can be found in Table 1.

2.1.1. Karlsruhe

Karlsruhe is in the state of Baden-Württemberg at 49°00′ N and 8°24′ E, 115 m above sea level and is the smaller of the two cities in respect to size and population (Table 1).

2.1.1.1. Geology, hydrogeology, and groundwater temperatures. Karlsruhe is located in the Upper Rhine Graben, a Cenozoic continental rift valley filled by Quaternary and Tertiary sediments. The Quaternary sediments with a varying thickness of around 150 m are dominated by sands and gravels showing minor contents of silts, clays and stones. The unsaturated zone of the study site consists mostly of sands and gravels (Geyer and Gwinner, 2011).

The upper aquifer has a thickness of up to 20 m, and the general groundwater flow direction is northwest towards the Rhine. In total, 82 groundwater monitoring wells in the study area are equipped with Ackermann WPS05 data loggers. These wells are continuously monitored by the Public Works Service Karlsruhe. Measurements of groundwater temperatures (GWT) and hydraulic heads are daily recorded (accuracy: 0.1 °C) at 7 AM at 2 to 3 m below the water surface. Well locations, weather station, and seasonal variability of GWT for three selected wells are exemplary shown in Fig. S1 (supporting information). To disregard the inter-annual variations in GWT and groundwater

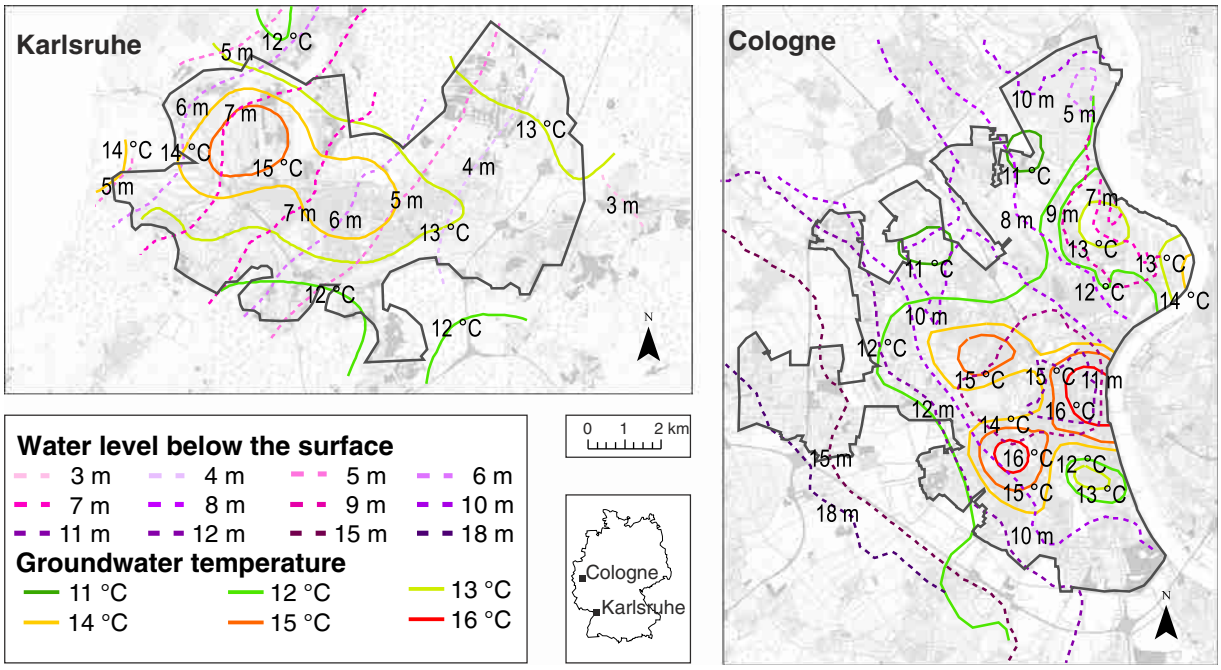

Fig. 1. Location of the study areas with annual mean groundwater level maps and annual mean groundwater temperature maps. Groundwater temperature in Karlsruhe was measured daily at about 9 m below the surface in 2011. The groundwater temperature in Cologne was measured at about 11 m below surface in 2009. Specific well locations are shown in Figs. S1 and S2 (Supplementary material).

depth, the mean annual GWT and groundwater levels of the annual cycle between March 2011 and 2012 are used in this study. Both GWT and groundwater level were interpolated by Menberg et al. (2013a,b) using kriging in GIS (ESRI® ArcInfo™ 10.0) and are shown in Fig. 1 with a resolution of 15 m × 15 m. The arithmetic mean of the GWT is 13.2 ± 1.3 °C. Its maximum is located northwest of the city center, where it reaches more than 16 °C. A second minor hot spot is located directly under the city center, where temperatures up to 15 °C were measured. The inner quantile range urban heat island intensity ($UHII_{90-10}$) that cuts the lowest and highest 10% of the temperatures before calculating the urban heat island intensity is 1.9 K (Menberg et al., 2013a).

The average groundwater depth is 5.4 ± 2.1 m below the surface. At its deepest points in the western part, the water table reaches 10.4 m below the surface, while the eastern area exhibits shallow groundwater at around 3 m below the surface.

2.1.1.2. Urban infrastructures. According to the GMES Urban Atlas, 83% of the study area in Karlsruhe is shaped by urban land use and consists of residential, commercial, and industrial units, roads and rail networks, etc. The overall building density is 21.0%, with the highest densities in the city center (Fig. 2).

Fig. 3 shows the sewage system and the district-heating network of Karlsruhe. The sewage system is a combined (rainwater and sanitary) system in the city center and a separate sewage system in the suburbs. The district heating network has been used since the early 19th century. Today, it is about 90 km long and connected to 23,500 households with an available power output of 25 PJ/a. In 2001, a survey performed by the newspaper for local economy (Zeitung für kommunale Wirtschaft, Zfk) showed that the heat loss is about 10%.

Geothermal applications, such as reinjection wells for industrial thermal wastewater, are also operating in Karlsruhe (Fig. 3). The current maximum licensed reinjection temperature is 20 °C (Hähnlein et al., 2010). In Karlsruhe about 4.5 Million m^3 of thermal wastewater are reinjected each year in 29 wells, altogether transporting slightly less than 0.1 PJ into the groundwater (Menberg et al., 2013b).

Table 1
General statistical information on both study areas. Note that the study area of Cologne covers only the western part of the city.

Study site	Karlsruhe	Cologne
Year of measurements	2011	2009
Area [km^2]	61.9	81.3
Building density [%]	21.0	21.6
Population	286,000[a]	485,000[b]
Mean air temperature [°C]	11.5[c]	11.4[c]
Mean ground surface temperature [°C]	14.4[d]	14.7[d]
Number of groundwater wells	82	73
Mean groundwater temperature [°C]	13.2	12.7
Mean groundwater depth [m]	5.4	10.2
Groundwater measurement depth [m below groundwater]	2–3	1

[a] Office for urban development, Karlsruhe (Stadt Karlsruhe, Amt für Stadtentwicklung).
[b] Office for urban development and statistics, Cologne (Stadt Köln, Amt für Stadtentwicklung und Statistik).
[c] German Weather Service (Deutscher Wetterdienst, DWD).
[d] Own calculations (see Section 2.2).

2.1.2. Cologne

Cologne is located in the state of North Rhine-Westphalia about 300 km further downstream along the Rhine. The city lies at 50°56′ N and 6°57′ E at 53 m above sea level. Due to the large number of observation wells needed for the spatial assessment of groundwater characteristics in this study, the study area is limited to the urban area on the western bank of the Rhine. It thus covers only about a quarter of the total city area.

2.1.2.1. Geology, hydrogeology, and groundwater temperatures. Cologne is located in the south of the Lower Rhine Basin. Above the Paleozoic bedrock are Tertiary and Quaternary layers. The shallow subsurface is composed of 15 to 25 m thick Pleistocene terrace deposits that, like in Karlsruhe, predominantly consist of gravels and sands (Balke, 1973).

The uppermost aquifer has a thickness of about 30 m and the general flow direction is northeast towards the receiving stream, the Rhine. GWT and groundwater levels (accuracy of 0.01 m) were measured in 73 groundwater wells between September and October 2009 using SEBA KLL-T logging equipment. GWTs were measured at 1 m below

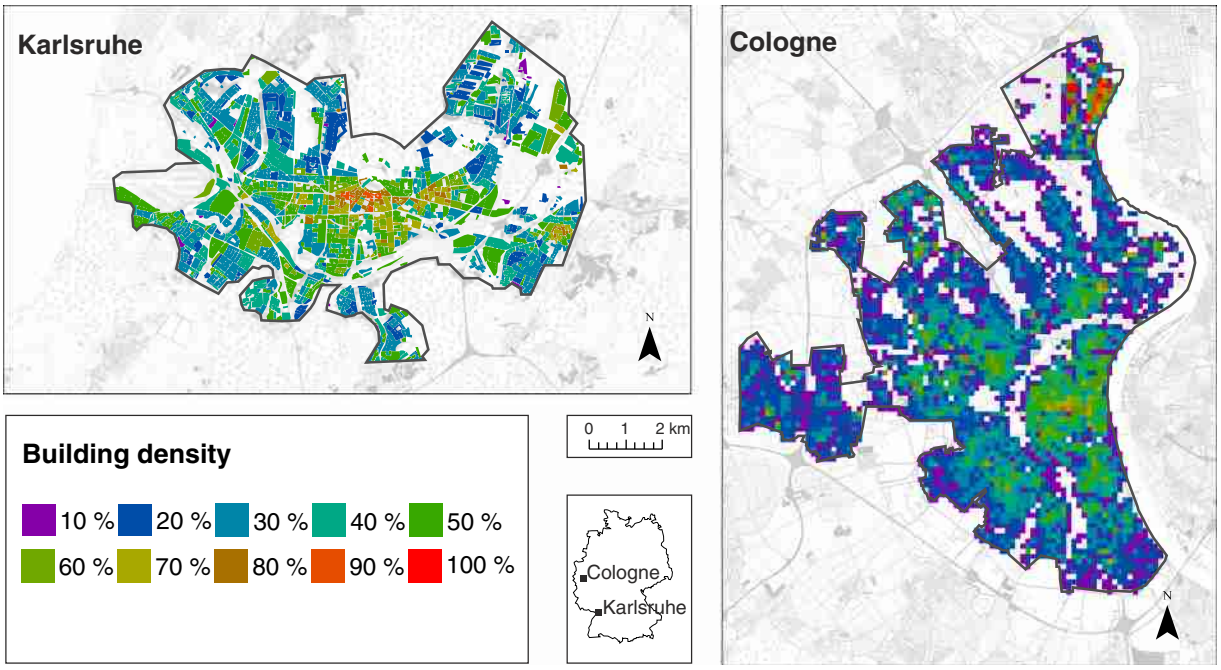

Fig. 2. Building density of Karlsruhe and Cologne.

the water table (approximately 11 m under the surface). At this depth the annual temperature variations are insignificant compared to the accuracy of 0.1 °C in most wells (Jung, 2013). The mean GWT is 12.7 ± 1.3 °C and the average observed groundwater level is 10.2 ± 6.1 m below the surface. GWT and depth were interpolated by Jung (2013) and Menberg et al. (2013a) using kriging (Table 1; Fig. 1). GWT in Cologne reaches a maximum of 16.2 °C in the city center under the main railway station. The $UHII_{10-90}$ is 2.1 K (Menberg et al., 2013a). The groundwater level in the northeast, close to the Rhine, is reaching up to 2 m below the surface, whereas it is 20 m below surface in the southwest of the city.

2.1.2.2. Urban infrastructures. In Cologne, 97% of the study area is shaped by urban land use (GMES Urban Atlas). Using the estate map of Cologne, the building density is estimated with 21.6% (Table 1). Again, the highest densities are found primarily in the city center, but also in industrial areas (Fig. 2). A subway system exists with about 19 km of underground rail inside the study area (Fig. 3). Although Cologne has

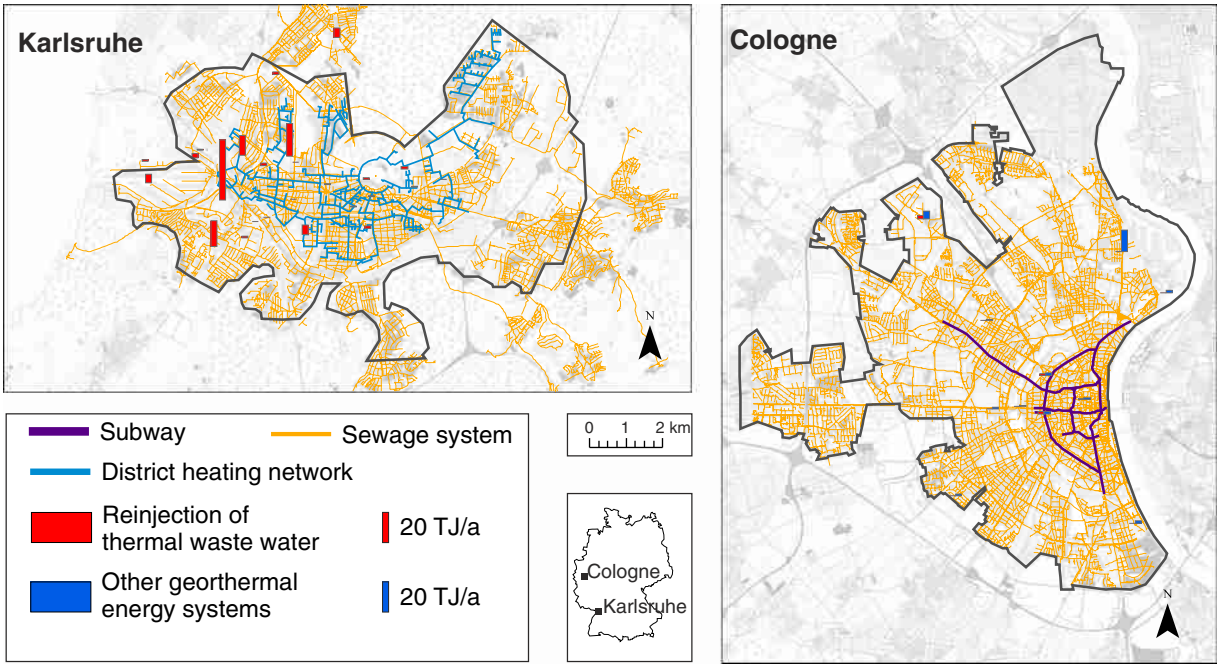

Fig. 3. Location of sewage-, district heating-, and subway systems in the study areas as well as the location of industrial reinjection wells of thermal wastewater and other geothermal energy systems such as GSHP and GWHP systems. As of 2011 Karlsruhe does not have a subway system. Information on the location of the district heating network in Cologne was not available.

a district heating network, no utility plan was accessible. However, its power output inside the study area (western bank) is 0.8 PJ/a with a heat loss of around 6% (Zfk, 2001).

While both reinjections of thermal wastewater and other geothermal energy systems, such as GSHP and GWHP systems, exist in Cologne, the latter are more frequent. Overall 33 TJ/a are extracted for heating inside the study area, while the cooling load only accounts for 6 TJ/a (Fig. 3).

2.2. Ground surface temperatures

Ground surface temperatures (GST) in both cities are determined according to the different surface materials within the urban environment and the characteristic deviation of the GST of these individual surface types from the ambient air temperature. Dědeček et al. (2012) measured the difference ΔT between ambient air temperature and GST for several surface types, such as grass surfaces (0.2–0.8 °C), sand and bare soil (1.5–2.0 °C), and asphalt (4.0–5.0 °C). We estimate the GST by adding these temperature differences to the air temperature according to the land use types within each city. The share of the different surface types in each individual land use type is adopted from the land use categorization of the Global Monitoring for Environment and Security (GMES) Urban Atlas (Table 2). Annual mean air temperatures are measured by the German Weather Service (Deutscher Wetterdienst, DWD). In both cities the meteorological stations are located at nearby airports (Figs. S1 and S2, Supplementary material). The average air temperature was 11.5 °C in Karlsruhe and 11.4 °C in Cologne. Unfortunately the spatial distribution of the air temperatures was not available and thus air temperature differences within the study areas had to be neglected. However, we believe them to be insignificant compared to the range of ΔT (Table 2).

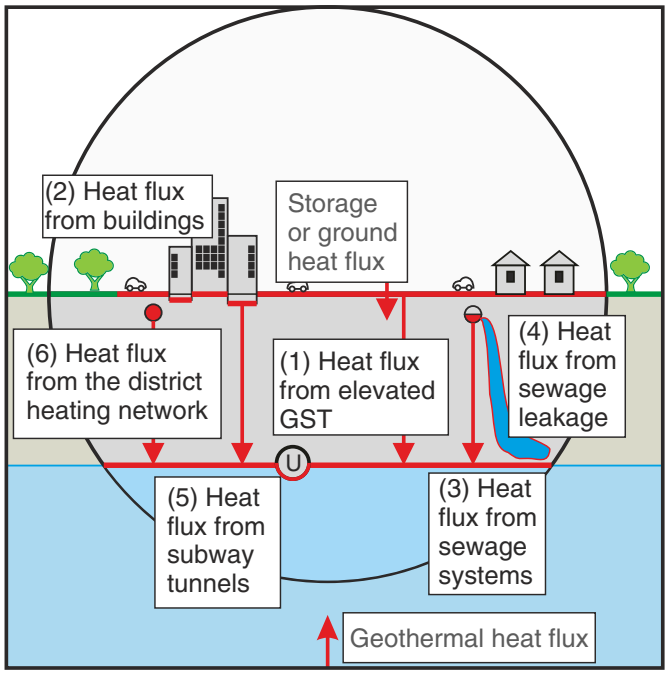

Fig. 4. Overview of the different studied heat fluxes: (1) heat flux from elevated ground surface temperatures (GST), (2) heat flux from buildings (i.e. basements), (3) heat flux from sewage systems, (4) heat flux from sewage leakage, (5) heat flux from subway tunnels, and (6) heat flux from district heating networks. The sum of the heat fluxes (1)–(6) represents the total anthropogenic heat flux into the subsurface (q_{tot}) determined in this study (Eq. (8)).

2.3. Mathematical modeling of the anthropogenic heat flux into the subsurface

2.3.1. Local anthropogenic heat flux model

Our heat flux model focuses on the unsaturated zone quantifying mean annual heat fluxes from the heat sources to the top of and therefore into the aquifer. In the unsaturated zone, temperature gradients and heat fluxes in the vertical direction are dominant (Taylor and Stefan, 2009). Hence, only vertical anthropogenic heat fluxes through the unsaturated zone are quantified. Fluxes from geothermal energy systems that interact directly and horizontally with the groundwater are not considered, yielding six heat sources for AHF_S: (1) elevated ground surface temperatures (GST), (2) basements (i.e. buildings), (3) sewage systems, (4) sewage leakage, (5) subway tunnels, and (6) district heating networks (see Fig. 4).

In this study, the regional anthropogenic heat flux model (Menberg et al., 2013b) was further developed. While still using a statistical and analytical approach, we introduce a local anthropogenic heat flux model, which analyzes all dominant heat fluxes spatially by determining them

Table 2
Assumed ground surface temperatures for different land uses.

Land-use description	Surface types[a] [%]			ΔT[b] [K]			Area covered [%]	
	Sand and bare soil	Grass	Asphalt	Min	Median	Max	Karlsruhe	Cologne
Forests	0	100	0	0.20	0.50	0.80	9.2	0.5
Green urban areas	0	100	0	0.20	0.50	0.80	7.9	7.6
Discontinuous very low density urban fabric (S.L. < 10%)	10	85	5	0.52	0.83	1.13	5.3	–
Agricultural + semi-natural areas + wetlands	50	50	0	0.85	1.13	1.40	0.0	3.2
Discontinuous low density urban fabric (S.L.: 10%–30%)	10	70	20	1.09	1.43	1.76	0.2	0.2
Construction sites	100	0	0	1.50	1.75	2.00	7.6	4.8
Mineral extraction and dump sites	100	0	0	1.50	1.75	2.00	0.9	0.7
Water bodies	100	0	0	1.50	1.75	2.00	0.9	0.4
Land without current use	100	0	0	1.50	1.75	2.00	0.1	0.0
Sports and leisure facilities	25	50	25	1.48	1.81	2.15	1.5	0.9
Railways and associated land	90	0	10	1.75	2.03	2.30	2.9	2.8
Discontinuous medium density urban fabric (S.L.: 30%–50%)	10	50	40	1.85	2.23	2.60	5.8	2.4
Discontinuous dense urban fabric (S.L.: 50%–80%)	10	25	65	2.80	3.23	3.65	15.6	18.8
Port areas	25	0	75	3.38	3.81	4.25	2.2	7.3
Continuous urban fabric (S.L. > 80%)	5	10	85	3.50	3.96	4.43	10.4	19.8
Industrial, commercial, public, military and private units	5	0	95	3.88	4.36	4.85	19.9	20.1
Isolated structures	0	0	100	4.00	4.50	5.00	1.5	0.3
Fast transit roads and associated land	0	0	100	4.00	4.50	5.00	0.1	–
Other roads and associated land	0	0	100	4.00	4.50	5.00	7.9	10.4

[a] GMES Urban Atlas.
[b] Dědeček et al. (2012); S.L.: sealing layer.

Table 3
Assumed parameter range distribution for the Monte Carlo simulation. Triangular distribution was used as a standard.

Heat flux process	Parameter	Name	Unit	Karlsruhe			Cologne		
				Minimum	Mode	Maximum	Minimum	Mode	Maximum
Increased GST	λ	Thermal conductivity [a]	W/mK	0.3	1	1.8	0.3	1	1.8
	T_{GS}^{ij}	Ground surface temperature	°C	See Table 2 and Fig. 5			See Table 2 and Fig. 5		
	T_{GW}^{ij}	Groundwater temperature	°C	See Fig. 1			See Fig. 1		
	δT_{GW}	Accuracy groundwater temperature	°C	−0.1	0	0.1	−0.1	0	0.1
	d_{GW}^{ij}	Groundwater depth	m	See Fig. 1			See Fig. 1		
	δd_{GW}	Accuracy groundwater depth	m	−0.01	0	0.01	−0.01	0	0.01
	bf^{ij}	Building density	%	See Fig. 2			See Fig. 2		
	δbf	Uncertainty of building density	%	−5	0	5	−5	0	5
Buildings	T_B	Temperature of basement/ground floor [b]	°C	15	17.5	20	15	17.5	20
	d_B	Basement depth	m	0	2.5	6	0	2.5	6
Sewage system	T_{SS}	Sewage temperature[c,d]	°C	12	18.5	25	10.33	17.59	26.8
	d_{SS}	Depth of sewage drains[e,d]	m	1	2	5	1	2	5
	D_{SS}	Diameter of sewage drains[f,d]	m	0.1	0.4	2	0.08	0.3	4.6
	l_{SS}	Length of sewage network[c,e,d]	m	770,000	880,000	990,000	907,051.5	1,007,835	1,108,618.5
Sewage leakage	c_{pSS}	Heat capacity of wastewater [c]	J/kgK	3708	4120	4532	3708	4120	4532
	ρ_{SS}	Density of wastewater[c]	kg/m^3	990	1100	1210	990	1100	1210
	V_{SS}	Annual wastewater volume[c,d]	m^3/a	33,997,000	35,707,500	37,418,000	48,873,592	49,000,000	50,873,592
	r_L	Leakage rate[f]	%	5	15	25	5	15	25
District heating	P_{DH}	Heat loss from district heating pipes[c,g]	MW	7.99	9.13	10.27	1.25	1.39	1.53
	r_d	Percentage heat flux directed downwards	%	25	37.5	50	25	37.5	50
	D_{DH}	Diameter of district heating pipes [f]	m	0.1	0.4	2	–	–	–
	l_{DH}	Length of district heating network	m	85,500	90,000	94,500	–	–	–
Subway system	T_{SW}	Subway system temperature[h]	°C	–	–	–	10	18.6	25.5
	l_{SW}	Length of subway system[h]	m	–	–	–	19,000	20,000	21,000
	D_{SW}	Diameter of subway system[h]	m	–	–	–	6.9	7	7.3
	t_{SW}	Thickness of subway tunnel walls [h]	m	–	–	–	–	1.1	–

[a] Menberg et al. (2013c), VDI 4640 (2010).
[b] DIN EN ISO 13370 (2008).
[c] Makurat (1980).
[d] Municipal drainage operator of Cologne (Köln, Stadtentwässerungsbetriebe).
[e] Civil engineering department Karlsruhe (Stadt Karlsruhe, Tiefbauamt).
[f] Eiswirth et al. (2002), Klinger (2007).
[g] Rheinenergie, 2011.
[h] Public transport company, Cologne (Kölner Verkehrsbetriebe, KVB).

for each pixel ij of the study area (resolution: 15 m × 15 m) individually. Thus, a spatially resolved heat flux map is obtained.

To account not only for the spatial variability, but also for uncertainties and the natural ranges of parameters, such as thermal conductivity and basement depth, a Monte Carlo (MC) approach with 800 iterations is employed to determine the fluxes in each pixel. The assumed parameter ranges used in the MC simulation are shown in Table 3. In all cases, a triangular distribution is chosen, defined by a minimum, a maximum and mode value stating the value with the highest probability. Where applicable, the parameter ranges previously applied by Menberg et al. (2013b) are also used here. In contrast to the previous work, we thus separate spatial variability (e.g. different groundwater temperatures in different pixels), from plain uncertainty (e.g. measurement accuracy), allowing a more accurate determination of heat fluxes and heat flow. In the following, both spatial variability and uncertainty will be expressed in the form of a standard deviation.

The model comprises three steps. First, the heat flux of all individual AHF_S sources in each pixel ij is determined using a Monte Carlo simulation. Second the anthropogenic heat flux per pixel ij is determined, which describes the average heat flux of the pixel. Third, the anthropogenic heat fluxes of all pixels are summed up to determine the heat flow, i.e. the energy amount transported into the aquifer over the whole study area in the span of one year.

2.3.2. Anthropogenic heat flux from individual sources

The anthropogenic heat flux from individual sources represents the energy per square meter and second that each AHF_S source transports into the groundwater. Most of the energy is transferred by conductive heat transport processes and can be determined using Fourier's law $|q| = \lambda \cdot \nabla T = \lambda \cdot \Delta T/\Delta d$. Here λ is the thermal conductivity and ∇T the thermal gradient that can be derived by dividing the difference in temperature ΔT by the distance Δd between two points. For the anthropogenic heat fluxes from elevated ground surface temperatures (q_{GST}) the temperature gradient depends on the difference between GST (T_{GS}) and GWT (T_{GW}) as well as on the depth d_{GW} of the water table (see Fig. 4). It can be calculated as follows:

$$q_{GST}^{ij} = \lambda \cdot \frac{T_{GS} - \left(T_{GW}^{ij} + \delta T_{GW}\right)}{d_{GW}^{ij} + \delta d_{GW}}. \quad (1)$$

Here δT_{GW} and δd_{GW} are the uncertainties of the measured value. The index ij indicates different values for different pixels ij. The assumed ranges can be found in Table 3. q_{GST} is determined for every pixel with a building density of less than 100%.

Anthropogenic heat fluxes from buildings (see Fig. 4) are calculated for each pixel ij with a building density of more than 0%. Here, the difference between the temperatures inside buildings/basements (T_B) and GWT, as well as the vertical distance between building depth (d_B) and groundwater depth, determine the thermal gradient, leading to the following equation:

$$q_{Bld}^{ij} = \lambda \cdot \frac{T_B - \left(T_{GW}^{ij} + \delta T_{GW}\right)}{\left(d_{GW}^{ij} + \delta d_{GW}\right) - d_B}. \quad (2)$$

Thermal insulation of buildings is not considered here, because in Germany, ground slab isolation was not implemented into construction regulations until the late 1990s (DIN 4108–2), leaving most buildings without insulation. Buildings that reach into the aquifer are still separated from the groundwater by the concrete slab of the basement. Thus, a

minimal distance between heat source and groundwater of 30 cm was assumed. Heat flux from basement walls was not considered.

Anthropogenic heat flux from the sewage system (see Fig. 4) is determined for every pixel, in which sewage drains are present. It comes in two ways: first, there is the conductive heat transfer (q_{SS}), represented again based on Fourier's law:

$$q_{SS}^{ij} = \lambda \cdot \frac{T_{SS} - \left(T_{GW}^{ij} + \delta T_{GW}\right)}{\left(d_{GW}^{ij} + \delta d_{GW}\right) - d_{SS}}. \quad (3)$$

Sewage pipes that reach into the aquifer are still separated from the groundwater by their mantle. Thus, a minimal distance between heat source and groundwater of 10 cm was assumed.

Second, there is an advective heat transfer representing sewage leakage (q_{SL}). To quantify the heat flux from sewage leakage, the energy content of the leaked water is estimated and divided by the area covered by the sewage system within the pixel:

$$q_{SL}^{ij} = c_{pSS}\rho_{SS}r_L \cdot \left[T_{SS} - \left(T_{GW}^{ij} + \delta T_{GW}\right)\right] \cdot \frac{V_{SS}}{l_{SS}D_{SS}}. \quad (4)$$

Here, c_{pSS} is the heat capacity of waste water, ρ_{SS} the density, r_L the leakage rate, V_{SS} the volume of wastewater, l_{SS} the length of the sewage system, and D_{SS} the diameter of the sewage system.

Anthropogenic heat fluxes originating from the subway system (see Fig. 4) are determined for all relevant pixels using Fourier's law. However, the subway tunnels in Cologne run under the groundwater level at around 19 m below surface (Kölner Verkehrsbetriebe, 2013). Hence, groundwater and heat source are merely separated by the tunnel walls with a thickness t_{SW} of 1.1 m:

$$q_{SW}^{ij} = \lambda \cdot \frac{T_{SW} - \left(T_{GW}^{ij} + \delta T_{GW}\right)}{t_{SW}}. \quad (5)$$

Anthropogenic heat flux from the district heating network (see Fig. 4) is determined for all relevant pixels. The downwards directed percentage r_d of the systems heat loss P_{DH} is taken and divided by the area covered by the district heating network leading to the following equation:

$$q_{DH}^{ij} = P_{DH} \cdot r_{DH} \cdot \frac{1}{l_{DH} \cdot D_{DH}} \quad (6)$$

Due to the chosen approach the heat flux from the district heating networks shows no spatial variability.

2.3.3. Anthropogenic heat flux per pixel

The anthropogenic heat flux $\overline{q}^{ij}$ per pixel is determined by scaling the anthropogenic heat fluxes of the individual sources to the reference area, i.e. the pixel size, of 15 m × 15 m. This is done for each heat source independently before the individual heat fluxes per pixel are added up to give the total heat flux of all anthropogenic heat sources for each pixel ij:

$$\overline{q}_{tot}^{ij} = \overbrace{q_{GST}^{ij} \cdot \left[1 - \left(bf^{ij} + \delta bf\right)\right]}^{\overline{q}_{GST}^{ij}} + \overbrace{q_{Bld}^{ij} \cdot \left(bf^{ij} + \delta bf\right)}^{\overline{q}_{Bld}^{ij}} + \overbrace{q_{SS}^{ij} \cdot \frac{l_{SS}D_{SS}}{A_{Pixel}N_{SS}}}^{\overline{q}_{SS}^{ij}} + \underbrace{q_{SL}^{ij} \cdot \frac{l_{SS}D_{SS}}{A_{Pixel}N_{SS}}}_{\overline{q}_{SL}^{ij}} + \underbrace{q_{SW}^{ij} \cdot \frac{l_{SW}D_{SW}}{A_{Pixel}N_{SW}}}_{\overline{q}_{SW}^{ij}} + \underbrace{q_{DH}^{ij} \cdot \frac{l_{DH}D_{DH}}{A_{Pixel}N_{DH}}}_{\overline{q}_{DH}^{ij}}. \quad (7)$$

To transfer the reference area to the pixel size, the building density (bf) is used for heat fluxes from increased GST and from buildings. For all other AHF_S sources, the heat fluxes per pixel are calculated by multiplying the anthropogenic heat fluxes with the fraction of the total area covered by the heat source (i.e. length l × diameter D), and the total area of the relevant pixels (area A_{Pixel} of one pixel × number N of relevant pixels).

2.3.4. Heat flow

The total anthropogenic heat flow into the subsurface I_{tot} is the energy input per year of the entire study area and is obtained by adding up the anthropogenic heat flux of every pixel as follows:

$$I_{tot} = A_{Pixel} \cdot \sum_{ij} \overline{q}_{tot}^{ij}. \quad (8)$$

In addition, the heat flow generated by each individual AHF_S source is determined accordingly.

2.4. Geothermal potential

The analysis of the geothermal potential Q/P_h offers a comparison of the potential heat content of the aquifer Q to the annual residential space heating demand P_h. The potential heat content of the aquifer is the geothermal heat content of the urban aquifer for a given temperature reduction ΔT. It can be estimated using the following equation (Balke, 1977; Zhu et al., 2010):

$$Q = Q_W + Q_S = A \cdot d \cdot n \cdot c_{p,W} \cdot \Delta T + A \cdot d \cdot (1-n) \cdot c_{p,s} \cdot \Delta T. \quad (9)$$

Here Q_W and Q_S are the potential heat contents of groundwater and solid respectively, A is the urban area, d is the aquifer thickness, n is the porosity of the aquifer, and $c_{p,W}$ and $c_{p,s}$ are the volumetric heat capacities of water and solid.

The annual residential space heating demand P_h is estimated as follows:

$$P_h = A_{LS} \cdot p \cdot q_{hd} \quad (10)$$

where A_{LS} is the average living space per person, p is the population and q_{hd} is the average annual unit heating demand (Zhu et al., 2010). The parameter values for both study sites are listed in Table 4.

In this study, we further introduce the sustainable geothermal potential I_{tot}/P_h that compares the annual anthropogenic heat input into the aquifer (i.e. the heat flow I_{tot} from above) to the annual residential space heating demand and hence, describes the capacity of sustainable energy usage.

3. Results and discussion

3.1. Ground surface temperatures

The results of the estimated GST are shown in Fig. 5 and Table 2. The mean GST in Karlsruhe is 14.4 °C and in Cologne 14.7 °C. This difference can be explained by a higher percentage of sealed areas in Cologne (Table 2).

3.2. Anthropogenic heat flux into the subsurface

3.2.1. Anthropogenic heat flux from individual sources

The results for the anthropogenic heat fluxes of all evaluated individual AHF_S sources are shown in Fig. 6 (and Table S1). The most dominant source of AHF_S is the district heating network in Karlsruhe with an average AHF_S of 62.8 W/m^2 and an uncertainty (in the form of standard deviation) of ±42.9 W/m^2, which is one order of magnitude more than fluxes from any other AHF_S source.

Increased GST is the least dominant source of anthropogenic heat flux with values of 0.24 ± 0.11 W/m^2 in Karlsruhe and 0.21 ± 0.06 W/m^2 in

Table 4
Assumed parameters for the estimation of the potential heat content of the aquifer and residential space heating demand.

Parameter	Name	Unit	Karlsruhe		Cologne	
			Mean	Uncertainty	Mean	Uncertainty
A	Urban area [a]	km^2	61.9	–	81.3	–
D	Aquifer thickness	m	30	20	20	10
N	Porosity of the aquifer	%	20	5	20	5
$c_{p,W}$	Volumetric heat capacity of water [b]	kJ/m^3K	4150	–	4150	–
$c_{p,S}$	Volumetric heat capacity of solid [b]	kJ/m^3K	2400	200	2150	50
ΔT	Temperature reduction [c]	K	4	–	4	–
Q	Potential heat content of the aquifer	PJ	20	14	17	9
A_{LS}	Average living space per person [d]	m^2	43	–	42.3	–
p	Population [s]	–	286,000	500	485,000	500
q_{hd}	Average annual heating demand [e]	kJ/m^2	525,600	180,000	525,600	180,000
P_h	Annual space heating demand	PJ	7	2	11	4
	Capacity for space heating	$Years^{-1}$	3.1	2.4	1.5	1.0

[a] See Table 1.
[b] VDI 4640 (2010).
[c] Zhu et al. (2010).
[d] Timm (2008).
[e] Nitsch (2002).

Cologne. Fluxes from increased GST correspond to the storage or ground heat fluxes (see Fig. 4) that are commonly used in literature to describe the energy balance of the surface. Storage heat fluxes in Basel, Switzerland, were measured hourly over the span of three days (8th, 25th and 26th June 2002) by Rigo and Parlow (2007). They found fluxes ranging from about −90 at night to 240 W/m^2 at daytime. Similarly Liebethal and Foken (2007) measured rural storage fluxes near Lindenberg in Germany on 10th June 2003 finding fluxes ranging from −50 at night to 150 W/m^2 around noon. While the here presented AHF_S from elevated GST fall within range of both of these studies, it is important to note that both studies analyzed only a short time frame in the summer month of June and are therefore expected to be elevated compared to the annual mean. A time series of 37 years of monthly measurements of storage heat flux in a rural site in Eastern Minnesota was presented by Baker and Baker (2002). Here the storage heat flux ranges between −6 and 6 W/m^2 at 1.6 m depth and is better comparable to our findings of annual flux from elevated GST through the entire unsaturated zone. Furthermore, in 2013 the Intergovernmental Panel on Climate Change (IPCC, 2013; Wild et al., 2013) analyzed a time frame of two decades. On a global scale, they estimated storage heat fluxes as the residual from the energy balance of the surface from 0.2 to 1.0 W/m^2, with the higher values representing fluxes into the ocean. This agrees well with our results for AHF_s from increased GST. In contrast, Beltrami et al. (2006) discussed the absorbed ground surface heat flux in the continental Northern Hemisphere using borehole temperature profiles of up to 400 m depth. They determined absorbed fluxes ranging from 0.025 to 0.075 W/m^2 in central Europe for the time period from 1930 to 1980.

The results for anthropogenic fluxes from buildings into the groundwater (3.61 ± 3.37 W/m^2 in Karlsruhe; 0.57 ± 0.47 W/m^2 in Cologne) are on the lower end of the fluxes through the ground floor slabs of a building, which range between 0 and 20 W/m^2 (Rees et al., 2000; Thomas and Rees, 1999). However, they agree well with the estimation of ~2 W/m^2 heat loss directly beneath a building (Ferguson and Woodbury, 2004). In Karlsruhe, fluxes from buildings as well as conductive fluxes from the sewage system (4.73 ± 6.72 W/m^2 in Karlsruhe; 0.94 ± 0.77 W/m^2 in Cologne) are significantly higher than in Cologne.

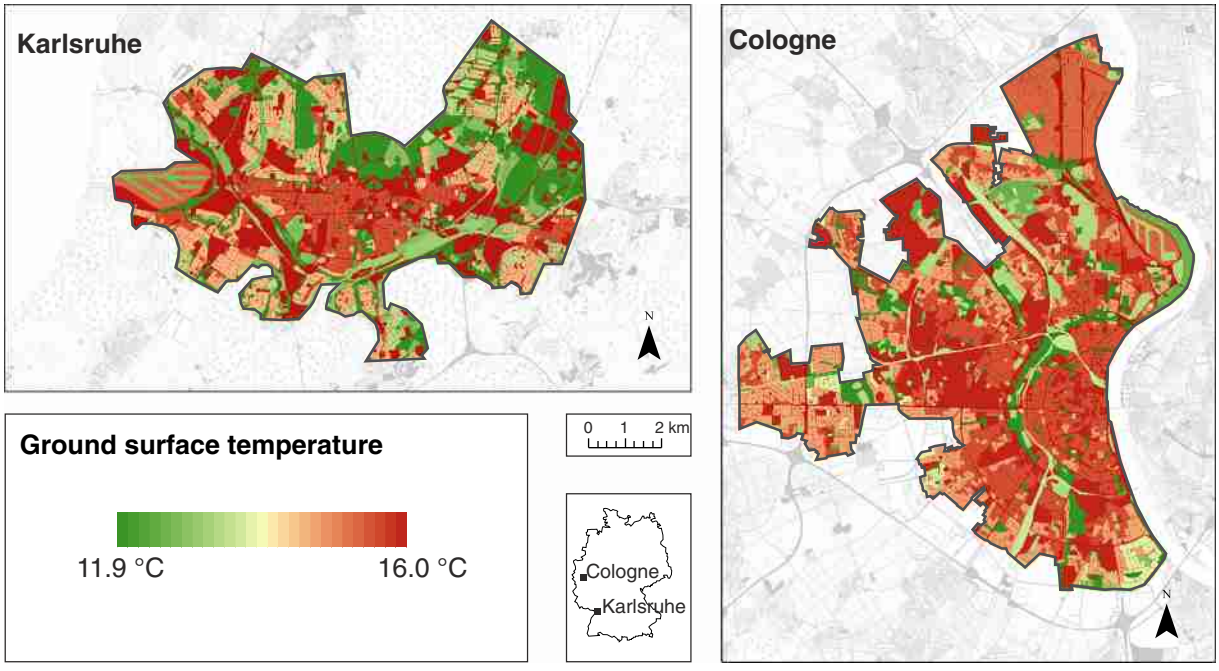

Fig. 5. Estimated mean ground surface temperatures (GST) in Karlsruhe and Cologne.

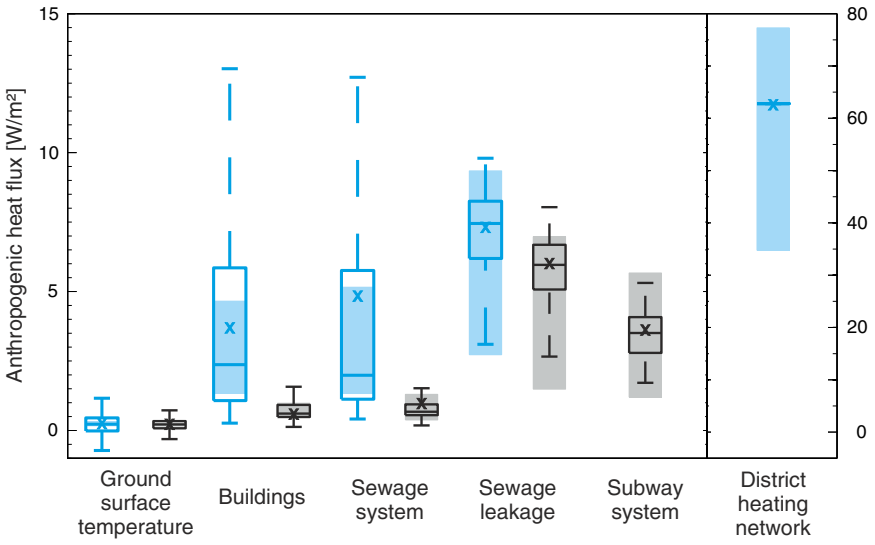

Fig. 6. Anthropogenic heat fluxes in Karlsruhe (blue) and Cologne (black) for all individual anthropogenic heat flux processes. Spatial variabilities are shown as boxplots, whereas the interquartile ranges of uncertainty are indicated by fully colored boxes. Mean values are indicated with a cross. (For interpretation of the references to color in this figure legend, the reader is referred to the web version of this article.)

This is also reflected in the long-tailed distribution of fluxes in Karlsruhe (Fig. 6), where 4% of all buildings and 15% of the sewage system generate fluxes above 10 W/m^2. In contrast in Cologne less than 0.01% of all fluxes from buildings and 1% of all conductive fluxes from sewage systems are above 10 W/m^2. The obvious explanation is that due to the higher groundwater levels in Karlsruhe 40% of all buildings and 1% of all sewage pipes are only 2 m above the groundwater level. Furthermore, 2% of all buildings reach into the groundwater, leaving the concrete slab of the basement (thickness: 30 cm) to separate groundwater and anthropogenic heat source. These marginal distances between groundwater and heat source lead to a high thermal gradient and therefore to a high anthropogenic heat flux. These findings corroborate the results for Basel, Switzerland, which show a dominant heat flux of 16 W/m^2 for buildings reaching into the groundwater, while other buildings generate fluxes of less than 1 W/m^2 (Epting et al., 2013). Furthermore, our models show that the anthropogenic heat flux from buildings in Karlsruhe can be decreased by 45% to 2.0 ± 0.8 W/m^2 (with a spatial variability of 1.8 W/m^2), if the assumed basement depth is reduced by only 0.4 m, following the model of Menberg et al. (2013b).

3.2.2. Anthropogenic heat flux per pixel

The anthropogenic heat flux of the average pixel is 1.10 W/m^2 for Karlsruhe and 0.39 W/m^2 for Cologne, respectively (Fig. 7 and Table S2). In contrast, the geothermal heat flux (see Fig. 4) in Karlsruhe is only about 0.08 W/m^2 (Cermak and Rybach, 1979) and in Cologne 0.06 W/m^2 (Balke, 1977), indicating that AHF_S dominate the heat flux into the urban aquifer.

Karlsruhe once again shows significantly higher fluxes and a wider distribution compared to Cologne. This is also reflected in the values of the standard deviation of both the spatial variability (1.49 W/m^2 in

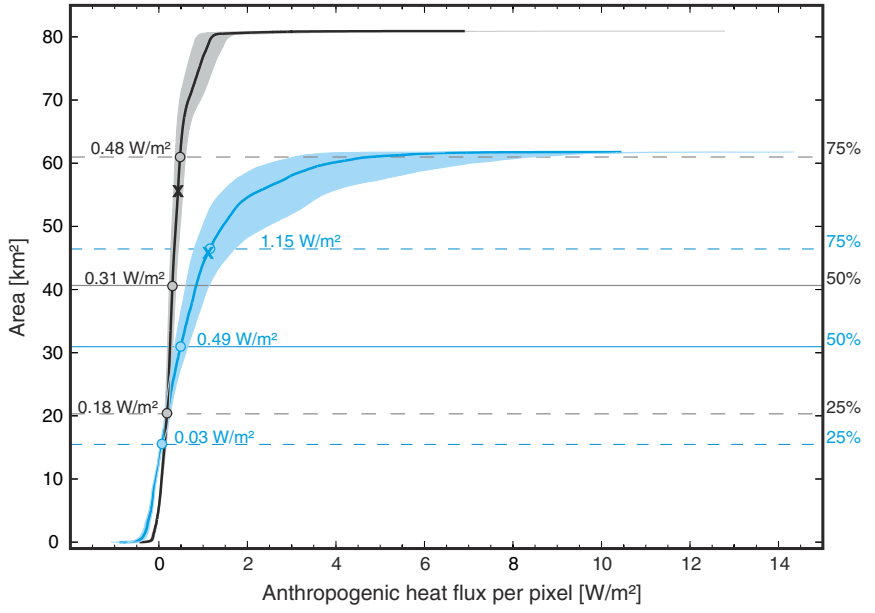

Fig. 7. Anthropogenic heat flux per pixel of Karlsruhe (blue) and Cologne (black). The spatial variability is shown as the cumulative plot, whereas the interquartile range of the uncertainty is colored. Median as well as 25th and 75th percentiles are further highlighted, the particular mean for each city is indicated with a cross. (For interpretation of the references to color in this figure legend, the reader is referred to the web version of this article.)

Karlsruhe; 0.38 W/m^2 in Cologne), as well as the uncertainty (0.73 W/m^2 in Karlsruhe; 0.12 W/m^2 in Cologne) of the results. The reason is the comparatively high groundwater level in Karlsruhe and the assigned uncertainty in the basement depth (0–6 m), which, in combination, result in a large and strongly variable thermal gradient, especially under buildings.

The spatial variability of the anthropogenic heat flux per pixel is depicted in Fig. 8. Cologne shows a comparatively homogeneous distribution with the highest fluxes along the subway line and next to the sewage network near the Rhine — in the area with the highest groundwater level. The northeast of Cologne reveals generally higher fluxes than the southwest, originating from a low groundwater temperature combined with elevated GST and again comparatively high groundwater levels. In this area, the largest GWHP system is installed with a heating load of 13.8 TJ/a. In this particular location, the heating efficiency of the geothermal installation is reduced by the low GWT, but at the same time, the sustainability of the system is increased through the high local AHFs.

The highest fluxes in Karlsruhe are found to the east of the city center, where groundwater levels are highest. In the western part, it is mostly the district-heating network that leads to particularly high heat fluxes. Negative AHF_S, i.e. fluxes from the groundwater to the surface, occur mainly in park areas, where the estimated ground surface temperature is lower than the groundwater temperature. Such green spaces are more common in Karlsruhe than in Cologne.

3.2.3. Heat flow

The sum of these upward directed fluxes accumulates to a median heat flow of −0.07 PJ/a in Karlsruhe and to only −0.01 PJ/a in the western part of Cologne. However, they are insignificant compared to the downward directed fluxes that accumulate to a median of 1.67 PJ/a in Karlsruhe and 0.95 PJ/a in Cologne. The overall energy balance is shown in Fig. 9 and Table S3. The mean of the total anthropogenic heat flow of Karlsruhe yields 2.1 ± 1.4 PJ/a, more than double that of Cologne (1.0 ± 0.3 PJ/a). The most dominant contributors of heat in Karlsruhe are buildings/basements with 1.5 ± 1.4 PJ/a. In Cologne, buildings generally do not reach into the groundwater and therefore only account for 0.3 ± 0.1 PJ/a. Nonetheless, they are the second most dominant AHF_S source. Although insignificant regarding the anthropogenic heat flux of all individual sources, increased ground surface temperatures (GST) are the most dominant contributor of anthropogenic heat flow in Cologne, with values of 0.4 ± 0.1 PJ/a due to the spatial extent of the affected areas. In Karlsruhe, fluxes from increased GST generate a heat flow of 0.3 ± 0.1 PJ/a, which represents the second largest source of anthropogenic heat flow in the groundwater. In contrast, fluxes caused by industrial reinjection of thermal waste water and other geothermal systems account for only 0.08 PJ/a in Karlsruhe and −0.03 PJ/a in Cologne (Jung, 2013; Menberg et al., 2013b).

Although being dominant regarding anthropogenic fluxes from individual sources, the district heating networks of each study area only account for a minor heat flow of 0.11 ± 0.02 PJ/a in Karlsruhe and 0.02 ± 0.01 PJ/a in Cologne, respectively (Table S3). For Karlsruhe, Menberg (2013) determined similar values with minor differences for the heat flow from buildings and from increased GST. This can easily be explained by the different estimations for basement depths and GST in both studies. Overall, the separation of spatial variability and uncertainty introduced in this study reduces the standard deviation of the total flow by 87% in comparison to the previous approach by Menberg (2013).

3.2.4. Covariance analysis

To analyze the model sensitivity in relation to the uncertainty of the Monte Carlo simulation, Spearman's rank correlation coefficients between the total heat flow and the parameter range distributions are determined (Fig. 9, Table 3). The results are illustrated in Fig. 10a); a detailed list of all parameters and their statistical significance p is given in Table S4 (supporting information). As expected, the uncertainty of basement depth shows the highest correlation to the heat flow in Karlsruhe, whereas it has only a minor influence on fluxes in Cologne, where buildings rarely reach into the groundwater.

Sewage temperature and the percentage of downwards directed heat flux show slightly elevated correlations in Cologne, confirming that the advective fluxes are more important in a city with a low thermal gradient. As expected, the heat flow of both cities is highly affected by the thermal conductivity, a parameter that is not expected to show a significant spatial variability in our study areas, due to the geological settings. However, since no measured values from within the study

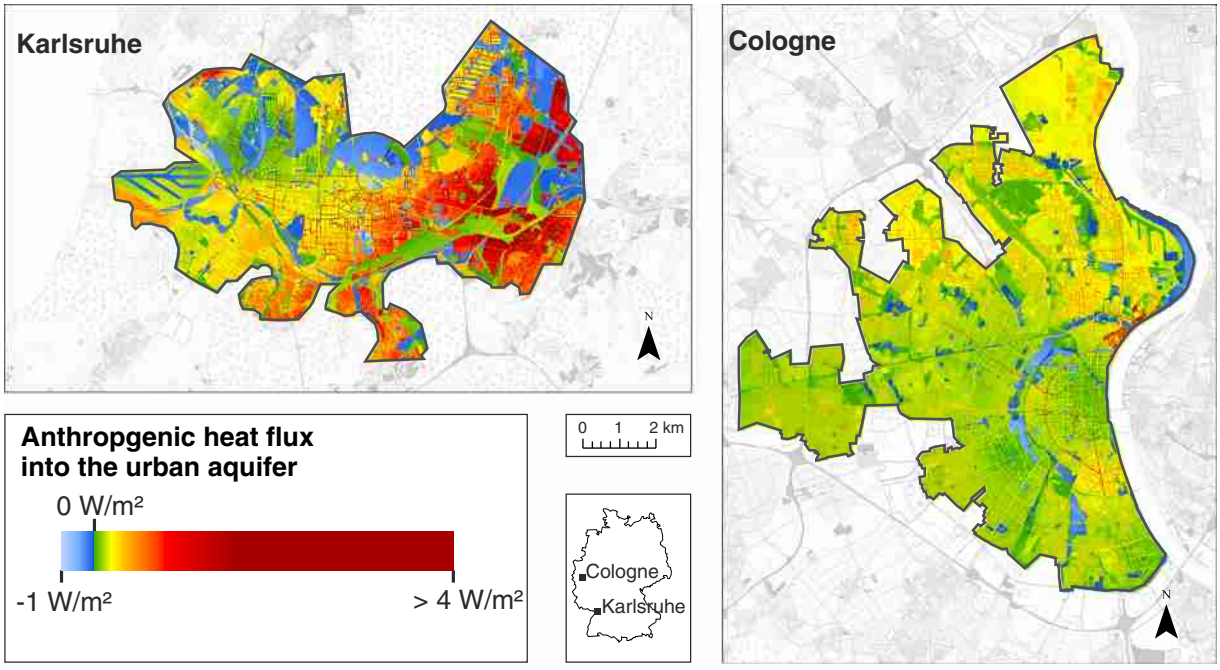

Fig. 8. Total anthropogenic heat flux per pixel into the groundwater of both study areas, Karlsruhe and Cologne. Negative fluxes indicate fluxes from groundwater to the surface. The spatial resolution is 15 m × 15 m.

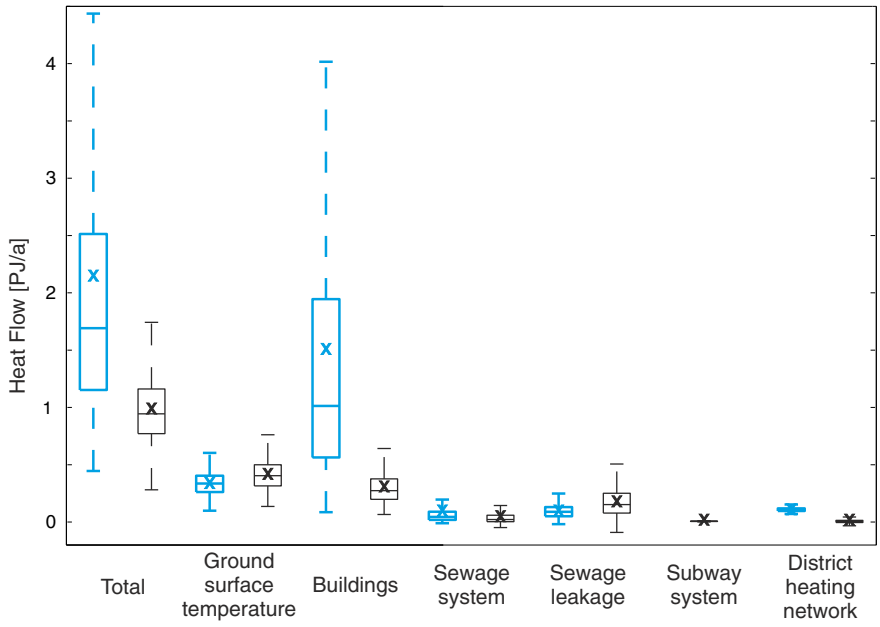

Fig. 9. Boxplot of the heat flow of Karlsruhe (blue) and of the western part of Cologne (black). Mean values are indicated with a cross. (For interpretation of the references to color in this figure legend, the reader is referred to the web version of this article.)

site were available, a broad range of 0.3 to 1.8 W/mK (Table 3) was chosen to account for all eventualities.

To analyze the model sensitivity in relation to the spatial variability of its input parameters, Spearman's rank correlation coefficients between the spatial variability of the total heat flux and the input parameters are determined (Figs. 1, 2, 4 and 8). The results are illustrated in Fig. 10b). A detailed list of all parameters and their statistical significance p is given in Table S5 (supporting information). The spatial variability of the thermal gradient $\nabla T = (T_{GS} - T_{GW})/d_{GW}$ is most influential regarding the spatial variability of the anthropogenic heat flux per pixel. However, nearly all uncertainties of the thermal gradient stem from the GST, which itself shows a high influence on the spatial variability of the anthropogenic heat flux per pixel. For further improvement of this method, it is therefore recommended to focus on spatial measurements of GST data in urban areas. Besides the thermal gradient and its linked parameters, building density is the most significant parameter.

3.3. Implications

Fig. 11 shows the potential heat content of the aquifer for a temperature reduction of 4 K, annual residential space heating demand and the annual anthropogenic heat flow determined for both study sites. The mean values and the uncertainties of the potential heat input as well as the annual heating demand are also given in Table 4. The heat content of the aquifer in Karlsruhe could provide enough heat to cover the space heating demand for 3.1 ± 2.4 years, while western Cologne's aquifer only yields heat for 1.5 ± 1 years. These differences in the geothermal potential stem from a thinner aquifer in Cologne in combination with a higher population and therefore higher space heating demand inside

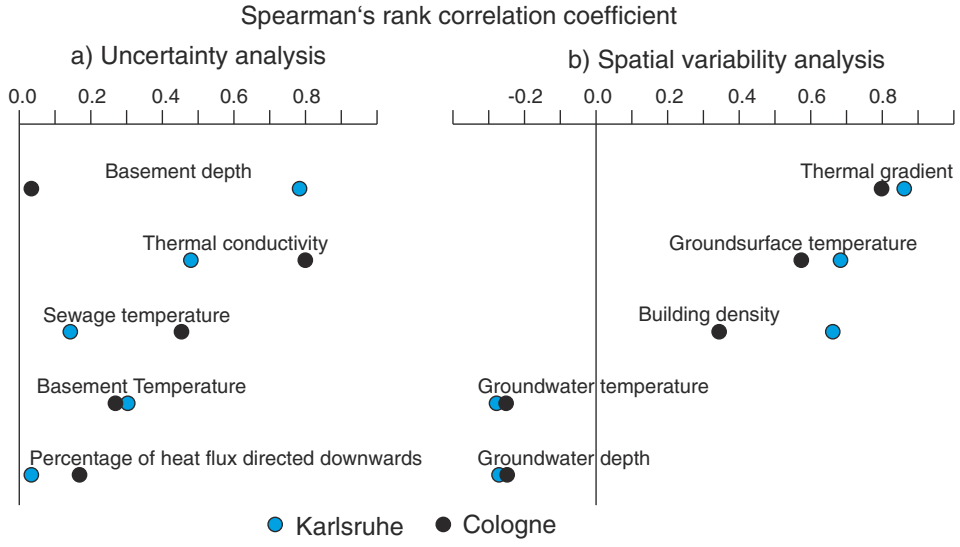

Fig. 10. Spearman's rank correlation coefficients between the heat flow and the individual parameters as an analysis of uncertainty, and between the heat flux per pixel and the individual parameters as an analysis of spatial variability. The thermal gradient ∇T was determined through: $\nabla T = (T_{GS} - T_{GW})/d_{GW}$. Only parameters with a correlation coefficient of >0.1 are shown. The statistical variance p can be found in the supporting information (Tables S4 and S5).

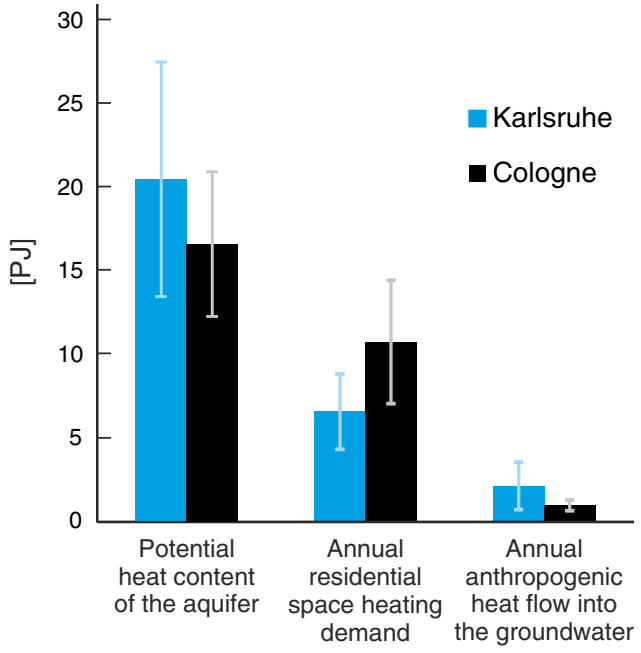

Fig. 11. Comparison of the determined anthropogenic heat flow with the annual residential space heating demand and the potential heat content of the aquifer for a temperature reduction of 4 K. Uncertainties are given in the form of standard deviations. Note that only the western part of Cologne is covered in this analysis.

the study area. An earlier study of the entire municipal Cologne showed a capacity for space heating in between 2.5 and 10.7 years for a temperature reduction of 2 to 6 K and assuming a rather optimistic average annual heating demand of 180,000 kJ/m^2 (Zhu et al., 2010). Furthermore, in Westminster, a large proportion of buildings could support their own heating demand using GSHPs without losing control of ground thermal capacity (Zhang et al., 2014). In Finland, 25% to 40% of annually constructed residential buildings could be heated utilizing groundwater (Arola et al., 2014). However, using the heat content of the aquifer for space heating will cool the urban aquifer by several degrees. In order to sustainably utilize the geothermal potential, the energy budget of all geothermal energy systems combined – heating and cooling – should not exceed the annual anthropogenic heat input into the aquifer. Nevertheless, assuming a steady-state system, this energy could sustainably supply 32% of the annual residential space heating demand in Karlsruhe and 9% in Cologne. This would be even more if additional cooling systems were to be installed. This also neglects that cooling of the ground would increase the conductive heat flux and thus the thermal replenishment of the aquifer. However, currently, a total of only about 0.03 PJ of heat are extracted in the study area of Cologne each year. This is merely 5% of the annual heat flow generated by AHF_S. In Karlsruhe, there are currently no significant industrial geothermal heating systems in place. On the contrary, 0.1 PJ of energy are transported into the groundwater each year mainly due to reinjection of thermal wastewater.

4. Conclusions

The development of a sustainable geothermal energy concept should be the goal of cities that want to use renewable energies such as shallow geothermal energy or thermally manage their groundwater resources. Here, a 2D statistical analytical heat flux model was developed and successfully applied to the cities of Karlsruhe and Cologne, Germany. The heat flux model gives a spatial representation of the vertical subsurface anthropogenic heat fluxes into urban aquifers. Hence, a sustainable thermal energy management tool could be developed for both cities.

We found that district heating pipes are the dominant source of anthropogenic heat fluxes with average values of more than 60 W/m^2, more than one order of magnitude higher than all other heat sources. Only sewage pipes and basements reaching into the groundwater are the cause of equally extraordinary heat sources with maximal fluxes of 40 W/m^2 and 14 W/m^2, respectively. These can be found in Karlsruhe, where the groundwater level is on average only 5.4 m below the subsurface. In the studied western part of Cologne, with a mean groundwater depth of 10.2 m, buildings and the sewage system do not reach into the groundwater. Thus, their fluxes show only minor spatial variability. Furthermore, in Cologne, the total AHF_S is lower (0.39 ± 0.12 W/m^2) and has a lower spatial variability (± 0.38 W/m^2) than the total AHF_S in Karlsruhe (1.10 ± 0.73 W/m^2; spatial variability of ± 1.49 W/m^2).

While dominating the local anthropogenic fluxes, the district heating network is insignificant for the citywide AHF_S budget in both cities. Heat from buildings (1.51 ± 1.36 PJ/a in Karlsruhe; 0.31 ± 0.14 PJ/a in western Cologne) and elevated GST (0.34 ± 0.10 PJ/a in Karlsruhe; 0.42 ± 0.13 PJ/a in western Cologne) are dominant contributors of the anthropogenic heat flow into the urban aquifer. In Karlsruhe, buildings are the source of 70% (in Cologne 30%) of the annual heat transported into the groundwater, which is mainly caused by buildings reaching into or close to the groundwater. A covariance analysis confirmed these findings. Hence, basement depth is the most influential factor to citywide heat flow in cities with a high groundwater level.

The spatial distribution of fluxes, however, is mostly influenced by the thermal gradient of the unsaturated zone. A cold GWT combined with a high GST, as well as a high groundwater level, results in elevated fluxes like in the east of Karlsruhe. Overall, 2.15 ± 1.42 PJ and 0.99 ± 0.32 PJ of thermal energy are annually transported into the groundwater of Karlsruhe and western Cologne due to AHF_S. This is sufficient to sustainably cover 32% and 9% of the annual residential space heating demand of Karlsruhe and western Cologne, respectively.

Acknowledgments

The financial support for S. Benz from the German Research Foundation (DFG) under grant number BL 1015/4-1 and the Swiss National Science Foundation (SNSF) under grant number 200021L 144288 is gratefully acknowledged. Furthermore, we thank Susanne Reimer, Friedhelm Fischer, Rüdiger Haas and Ralf Schneider (Tiefbauamt Karlsruhe), Annette März (Stadt Karlsruhe, Umwelt-und Arbeitsschutz), and Manuel Rink (Stadtwerke Karlsruhe GmbH) as well as Sebastian Greve (Stadtentwässerungsbetriebe Köln), Stephanie Kempkes (Landesamt für Natur, Umwelt und Verbraucherschutz NRW), Karin Landsberg (Bezirksregierung Köln), and Stefan Simon (Erft-Verband) for their valuable support with data and additional information. Finally, we would like to thank the four anonymous reviewers for their comments.

Appendix A. Supplementary data

Supplementary data to this article can be found online at http://dx.doi.org/10.1016/j.scitotenv.2015.04.003.

References

Allen, A., Milenic, D., Sikora, P., 2003. Shallow gravel aquifers and the urban 'heat island' effect: a source of low enthalpy geothermal energy. Geothermics 32, 569–578.
Allen, L., Lindberg, F., Grimmond, C.S.B., 2011. Global to city scale urban anthropogenic heat flux: model and variability. Int. J. Climatol. 31, 1990–2005.
Arola, T., Korkka-Niemi, K., 2014. The effect of urban heat islands on geothermal potential: examples from Quaternary aquifers in Finland. Hydrogeol. J. 22, 1953–1967.
Arola, T., Eskola, L., Hellen, J., Korkka-Niemi, K., 2014. Mapping the low enthalpy geothermal potential of shallow Quaternary aquifers in Finland. Geotherm. Energy 2, 1–20.
Baker, J.M., Baker, D.G., 2002. Long-term ground heat flux and heat storage at a mid-latitude site. Clim. Chang. 54, 295–303.
Balke, K.D., 1973. Geothermische und hydrogeologische Untersuchungen in der südlichen Niederrheinischen Bucht. Bundesanstalt für Bodenforschung und den Geologischen Landesämtern der Bundesrepublik Deutschland, Hannover.
Balke, K.D., 1977. Das Grundwasser als Energieträger. Brennstoff-Wärme-Kraft 29.

Bayer, P., Saner, D., Bolay, S., Rybach, L., Blum, P., 2012. Greenhouse gas emission savings of ground source heat pump systems in Europe: a review. Renew. Sust. Energ. Rev. 16, 1256–1267.

Beltrami, H., Ferguson, G., Harris, R.N., 2005. Long-term tracking of climate change by underground temperatures. Geophys. Res. Lett. 32, 1–4.

Beltrami, H., Bourlon, E., Kellman, L., González-Rouco, J.F., 2006. Spatial patterns of ground heat gain in the Northern Hemisphere. Geophys. Res. Lett. 33.

Blum, P., Campillo, G., Münch, W., Kölbel, T., 2010. CO_2 savings of ground source heat pump systems — a regional analysis. Renew. Energy 35, 122–127.

Bowler, D.E., Buyung-Ali, L., Knight, T.M., Pullin, A.S., 2010. Urban greening to cool towns and cities: a systematic review of the empirical evidence. Landsc. Urban Plan. 97, 147–155.

Cermak, V., Rybach, L., 1979. Terrestrial heat flow in Europe. Springer Verlag, Heidelberg-Berlin, Germany.

Dědeček, P., Šafanda, J., Rajver, D., 2012. Detection and quantification of local anthropogenic and regional climatic transient signals in temperature logs from Czechia and Slovenia. Clim. Chang. 113, 787–801.

Deutscher Wetterdienst (DWD),). Web-based weather request and distribution systemhttp://www.dwd.de/ (accessed May 20, 2014).

Deutsches Institut für Normung e.V. DIN 4108-2, 2011. Wärmeschutz und Energie-Einsparung in Gebäuden — Teil 2: Mindestanforderungen an den Wärmeschutz (Thermal protection and energy economy in buildings — Part 2: Minimum requirements to thermal insulation). Beuth Verlag GmbH, Berlin.

Deutsches Institut für Normung e.V. DIN EN ISO 13370, 2008. Wärmetechnisches Verhalten von Gebäude — Wärmeübertragung über das Erdreich (Thermal performance of buildings — Heat transfer via the ground). Beuth Verlag GmbH, Berlin.

Eggleston, J., McCoy, K.J., 2014. Assessing the magnitude and timing of anthropogenic warming of a shallow aquifer: example from Virginia Beach, USA. Hydrogeol. J. 23, 105–120.

Eiswirth, M., Held, I., Hötzl, H., Wolf, L., 2002. Abwasser im urbanen Grundwasserleiter: Stoffeintrag, Umsetzung und Gefährdungspotential. Progress Report, Gorschergruppe Kanalleckage: Gefährdungspotential von Abwasser aus undichten Kanälen für Boden und Grundwasser. Universität Karlsruhe (TH), Karlsruhe, Germany.

Epting, J., Handel, F., Huggenberger, P., 2013. Thermal management of an unconsolidated shallow urban groundwater body. Hydrol. Earth Syst. Sci. 17, 1851–1869.

Ferguson, G., Woodbury, A.D., 2004. Subsurface heat flow in an urban environment. J. Geophys. Res. Solid Earth 109 (B02402), 1–9.

Ferguson, G., Woodbury, A.D., 2007. Urban heat island in the subsurface. Geophys. Res. Lett. 34, L23713.

Gabriel, K.M., Endlicher, W.R., 2011. Urban and rural mortality rates during heat waves in Berlin and Brandenburg, Germany. Environ. Pollut. 159, 2044–2050.

Geyer, O.F., Gwinner, M.P., 2011. Geologie von Baden-Württemberg. Schweizerbart, Stuttgart.

Global Monitoring for environment and security (GMES), European Environment Agency: Urban Atlas (http://www.eea.europa.eu/data-and-maps/data/urban-atlas) (access January 19, 2015)

Hähnlein, S., Bayer, P., Blum, P., 2010. International legal status of the use of shallow geothermal energy. Renew. Sustain. Energy Rev. 14, 2611–2625.

Hähnlein, S., Bayer, P., Ferguson, G., Blum, P., 2013. Sustainability and policy for the thermal use of shallow geothermal energy. Energy Policy 59, 914–925.

Headon, J., Banks, D., Waters, A., Robinson, V.K., 2009. Regional distribution of ground temperature in the Chalk aquifer of London, UK. Q. J. Eng. Geol. Hydrogeol. 42, 313–323.

Herbert, A., Arthur, S., Chillingworth, G., 2013. Thermal modelling of large scale exploitation of ground source energy in urban aquifers as a resource management tool. Appl. Energy 109, 94–103.

Hötzl, H., Makurat, A., 1981. Veränderungen der Grundwassertemperaturen unter dicht bebauten Flächen am Beispiel der Stadt Karlsruhe. Z. Dtsch. Geol. Ges. 132, 767–777.

Ichinose, T., Shimodozono, K., Hanaki, K., 1999. Impact of anthropogenic heat on urban climate in Tokyo. Atmos. Environ. 33, 3897–3909.

IPCC, 2013. Climate change 2013: the physical science basis. In: Stocker, T.F., Qin, D., Plattner, G.-K., Tignor, M., Allen, S.K., Boschung, J., Nauels, A., Xia, Y., Bex, V., Midgley, P.M. (Eds.), Contribution of Working Group I to the Fifth Assessment Report of the Intergovernmental Panel on Climate Change. Cambridge University Press, Cambridge, United Kingdom and New York, NY, USA http://dx.doi.org/10.1017/CBO9781107415324 (1535 pp.).

Jauregui, E., 1997. Heat island development in Mexico City. Atmos. Environ. 31, 3821–3831.

Jung, S., 2013. Wärmefluss in der urbanen Wärmeinsel Köln.

Kertesz, R., Sansalone, J., 2014. Hydrologic transport of thermal energy from pavement. J. Environ. Eng. 140.

Klinger, J., 2007. Beschreibung der Wasser- und Stoffflüsse in einem urbanen Raum unter besonderer Berücksichtigung von Kanalleckagen. (Ph.D). Universität Karlsruhe (TH), Karlsruhe, Germany.

Kollet, S.J., Cvijanovic, I., Schuttemeyer, D., Maxwell, R.M., Moene, A.F., Bayer, P., 2009. The influence of rain sensible heat and subsurface energy transport on the energy balance at the land surface. Vadose Zone J. 8, 846–857.

Köln, Stadtentwässerungsbetriebe, e. Einzugsgebiete der Kläranlagen, Kölnhttp://www.steb- koeln.de /klaeranlagen.html (accessed: January 09, 2013).

Kölner Verkehrsbetriebe (KVB),). http://www.nord-sued-stadtbahn.de (accessed: May 15., 2013).

Li, D., Bou-Zeid, E., 2014. Quality and sensitivity of high-resolution numerical simulation of urban heat islands. Environ. Res. Lett. 9.

Liebethal, C., Foken, T., 2007. Evaluation of six parameterization approaches for the ground heat flux. Theor. Appl. Climatol. 88, 43–56.

Lubis, R.F., Yamano, M., Delinom, R., Martosuparno, S., Sakura, Y., Goto, S., et al., 2013. Assessment of urban groundwater heat contaminant in Jakarta, Indonesia. Environ. Earth Scie. 70, 2033–2038.

Makurat, A., 1980. Analyse der Temperaturschwankungen des Grundwassers im Stadtgebiet von Karlsruhe. (Diploma Thesis). Universität Karlsruhe (TH), Karlsruhe, Germany.

Menberg, K., 2013. Anthropogenic and natural alterations of shallow groundwater temperatures. (PhD). Karlsruhe Institute of Technology (KIT); Karlsruhe, Germany.

Menberg, K., Bayer, P., Zosseder, K., Rumohr, S., Blum, P., 2013a. Subsurface urban heat islands in German cities. Sci. Total Environ. 442, 123–133.

Menberg, K., Blum, P., Schaffitel, A., Bayer, P., 2013b. Long-term evolution of anthropogenic heat fluxes into a subsurface urban heat island. Environ. Sci. Technol. 47, 9747–9755.

Menberg, K., Steger, H., Zorn, R., Reuss, M., Proll, M., Bayer, P., et al., 2013c. Determination of thermal conductivity in the subsurface using laboratory and field experiments and theoretical models. Grundwasser 18, 103–116.

Muller, N., Kuttler, W., Barlag, A.B., 2014. Analysis of the subsurface urban heat island in Oberhausen, Germany. Clim. Res. 58, 247–256.

Nitsch, J., 2002. Struktur und Entwicklung der zukünftigen Stromversorgung Baden-Württembergs. Arbeitsgemeinschaft DLR/ISI/ZSW.

Oke, T.R., 1973. City size and the urban heat island. Atmos. Environ. 7, 769–779.

Peng, S., Piao, S., Ciais, P., Friedlingstein, P., Ottle, C., Bréon, F.-M., et al., 2012. Surface urban heat island across 419 global big cities. Environ. Sci. Technol. 46, 696–703.

Rees, S.W., Thomas, H.R., Zhou, Z., 2000. Ground heat transfer: some further insights into the influence of three-dimensional effects. Build. Serv. Eng. Res. Technol. 21, 233–239.

Rheinenergie, A.G., 2011. Geschäftsbericht (Daten des Fernwärmenetzes). http://www.rheinenergie.com/de/unternehmensportal/ueber_uns/rheinenergie/geschaeftsberichte/index.php (accessed May 23, 2013).

Rigo, G., Parlow, E., 2007. Modelling the ground heat flux of an urban area using remote sensing data. Theor. Appl. Climatol. 90, 185–199.

Sailor, D.J., Lu, L., 2004. A top-down methodology for developing diurnal and seasonal anthropogenic heating profiles for urban areas. Atmos. Environ. 38, 2737–2748.

Santamouris, M., Papanikolaou, N., Livada, I., Koronakis, I., Georgakis, C., Argiriou, A., et al., 2001. On the impact of urban climate on the energy consuption of building. Sol. Energy 70, 201–216.

Sarrat, C., Lemonsu, A., Masson, V., Guedalia, D., 2006. Impact of urban heat island on regional atmospheric pollution. Atmos. Environ. 40, 1743–1758.

Stadt Karlsruhe, e. Tiefbauamt Karlsruhe: Die Stadtentwässerung in Karlsruhehttp://www.karlsruhe.de/b3/bauen/tiefbau/entwaesserung/entwaesserungsgebuehr/HF_sections/content/ZZk9uVuzOo24XJ/ZZk9uWfqOuhpKP/Tiefbauamt_Broschuere_2010.pdf (accessed March 20, 2013).

Stadt Karlsruhe, e. Amt für Stadtentwicklung: Statistisches Jahrbuch 2012http://web1.karlsruhe.de/Stadtentwicklung/siska/pdf/Jahrbuch2012.pdf (accessed January 19, 2015).

Stadt Köln, n. Amt für Stadtentwicklung und Statistik: Kölner Stadtteilinformationen — Zahlen 2010http://www.stadt-koeln.de/mediaasset/content/pdf15/stadtteilinformationen_2010.pdf (accessed January 19, 2015).

Taha, H., 1997. Urban climates and heat islands: albedo, evapotranspiration, and anthropogenic heat. Energy Build. 25, 99–103.

Taniguchi, M., Uemura, T., Jago-on, K., 2007. Combined effects of urbanization and global warming on subsurface temperature in four Asian cities. Vadose Zone J. 6, 591–596.

Taniguchi, M., Shimada, J., Fukuda, Y., Yamano, M., Onodera, S., Kaneko, S., et al., 2009. Anthropogenic effects on the subsurface thermal and groundwater environments in Osaka, Japan and Bangkok, Thailand. Sci. Total Environ. 407, 3153–3164.

Taylor, C.A., Stefan, H.G., 2009. Shallow groundwater temperature response to climate change and urbanization. J. Hydrol. 375, 601–612.

Thomas, H.R., Rees, S.W., 1999. The thermal performance of ground floor slabs — a full scale in-situ experiment. Build. Environ. 34, 139–164.

Timm, U., 2008. Wohnsituation in Deutschland 2006 — Ergebnisse der Mikrozensus-Zusatzerhebung. In: Bundesamt, S. (Ed.), Wirtschaft und Statistik, p. 2.

Verein Deutscher Ingenieure (VDI), 2010. Thermische Nutzung des Untergrunds: Grundlagen, Genehmigungen, Umweltaspekte (Thermal use of the underground: Fundamentals, approvals, environmental aspects).VDI 4640. Beuth Verlag GmbH, Berlin.

Wild, M., Folini, D., Schär, C., Loeb, N., Dutton, E., König-Langlo, G., 2013. The global energy balance from a surface perspective. Clim. Dyn. 40, 3107–3134.

Yalcin, T., Yetemen, O., 2009. Local warming of groundwaters caused by the urban heat island effect in Istanbul, Turkey. Hydrogeol. J. 17, 1247–1255.

Zeitung für kommunale Wirtschaft (Zfk), 2001. Fernwärmeumfrage. Energieverluste aus dem Fernwärmenetz. http://zfk.ve.m-online.net/navframe/umfrage01.pdf (accessed: May 23, 2013).

Zhang, Y., Choudhary, R., Soga, K., 2014. Shallow geothermal energy application with GSHPs at city scale: study on the City of Westminster. Géotech. Lett. 4, 125–131.

Zhu, K., Blum, P., Ferguson, G., Balke, K.D., Bayer, P., 2010. The geothermal potential of urban heat islands. Environ. Res. Lett. 5 (art. no. 044002).

Zhu, K., Bayer, P., Grathwohl, P., Blum, P., 2014. Groundwater temperature evolution in the subsurface urban heat island of Cologne, Germany. Hydrol. Process. 29, 965–978.